A Bitopic Miniprotein Regulates a Membrane-Embedded Enzyme via Topological Allostery

Daniel K. Weber[1], Máximo Sanz-Hernández[2], U. Venkateswara Reddy[1], Songlin Wang[1], Erik K. Larsen[2], Tata Gopinath[1], Martin Gustavsson[1], Razvan L. Cornea[1], David D. Thomas[1] Alfonso De Simone[3] and Gianluigi Veglia[1,2,*]

[1] Department of Biochemistry, Molecular Biology, and Biophysics, University of Minnesota, Minneapolis, MN 55455, USA
[2] Department of Chemistry, University of Minnesota, Minneapolis, MN 55455, USA
[3] Department of Life Sciences, Imperial College London, South Kensington, London, SW7 2AZ, UK

[*] To whom correspondence should be addressed:

Gianluigi Veglia,
Department of Biochemistry, Molecular Biology & Biophysics,
University of Minnesota, 6-155 Jackson Hall, MN 55455.
Telephone: (612) 625-0758.
Fax: (612) 625-2163.
E-mail: vegli001@umn.edu.

Keywords: *Topological Allostery, membrane proteins, allosteric coupling, oriented solid-state NMR, bicelles.*

Phospholamban (PLN) is a mini-membrane protein that directly controls the cardiac Ca^{2+}-transport response to β-adrenergic stimulation, thus modulating cardiac output during the fight-or-flight response. In the sarcoplasmic reticulum membrane, PLN binds to the sarco(endo)plasmic reticulum Ca^{2+}-ATPase (SERCA), keeping this enzyme's function within a narrow physiological window. PLN phosphorylation or increase in Ca^{2+} concentration reverses the inhibitory effects. Despite a plethora of X-ray studies, the structural mechanism of SERCA regulation by PLN remains unknown. Using solid-state NMR spectroscopy and replica-averaged NMR-restrained structural refinement, we found that the transmembrane region of PLN is in equilibrium between inhibitory and non-inhibitory topologies within SERCA's binding groove. Phosphorylation of PLN at Ser16, or increase in Ca^{2+} concentration, shifts the equilibrium toward the non-inhibitory topologies, augmenting Ca^{2+} transport and muscle contractility. This type of allosteric regulation, via topological changes (topological allostery), may constitute a general mechanism for the other regulins that modulate SERCA activity in cardiac and skeletal muscle.

Miniproteins are translated from small open reading frames of 100-300 nucleotides in length and constitute a neglected part of the human proteome[1]. Most miniproteins are membrane-embedded and act as regulators or ancillary proteins to enzymes or receptors[2-4]. Among the most critical miniproteins is phospholamban (PLN), a bitopic membrane polypeptide that regulates the function of the sarco(endo)plasmic reticulum Ca^{2+}-ATPase (SERCA) in cardiac muscle[5]. PLN directly controls cardiac output by maintaining SERCA's activity within a tight physiological window[6]. SERCA is a ten-transmembrane (TM) pump that promotes diastole by removing Ca^{2+} from the sarcoplasm and restoring high Ca^{2+} concentrations in the sarcoplasmic reticulum (SR) in preparation for the next systole[6]. As with other P-type ATPases, SERCA is fueled by ATP and cycles between two major conformational states *E*1

and *E*2, of high and low Ca^{2+}-affinity, respectively[7]. In cardiomyocytes, PLN is expressed in 4-fold molar excess of SERCA, suggesting that this endogenous regulator is permanently bound to the enzyme in a 1:1 stoichiometric ratio[8]. PLN binds the ATPase *via* intramembrane protein-protein interactions, lowering its apparent Ca^{2+} affinity and stabilizing the *E*2 state of the pump[6,9]. SERCA/PLN inhibitory interactions are relieved upon β-adrenergic stimulation, which unleashes cAMP-dependent protein kinase A to phosphorylate PLN's cytoplasmic domain at Ser16, enhancing Ca^{2+} transport by SERCA and augmenting heart muscle contractility[10]. Ablation, point mutations, or truncations of PLN have been linked to congenital heart disease[9]. Despite multiple crystal structures of SERCA[7] and several structural studies of PLN free and bound to SERCA[11-13], the inhibitory mechanism of PLN and its reversal upon phosphorylation or Ca^{2+} increase are still unknown. Mutagenesis data and molecular modeling suggested that the regulation of SERCA occurs through electrostatic and hydrophobic interactions between the helical transmembrane (TM) region of PLN and the binding groove of the ATPase formed by TM2, TM6, and TM9[14]. Upon binding SERCA, however, the helical TM domain of PLN does not undergo significant changes in secondary structure[15,16]. As a result, X-ray crystallography[16] and other structural techniques (*e.g.*, EPR or NMR) have not offered significant mechanistic insights into the regulatory process.

Here, we reveal the elusive *topological changes* that are responsible for triggering PLN inhibition of SERCA (and its reversal), using a combination of oriented-sample solid-state NMR (OS-ssNMR) spectroscopy and dynamic structural refinement by replica-averaged orientational-restrained molecular dynamics simulations (RAOR-MD)[17,18]. The analysis of anisotropic ^{15}N chemical shifts (CSs) and ^{15}N-^{1}H dipolar couplings (DCs) of the SERCA/PLN complex reconstituted in magnetically aligned lipid bicelles unveiled PLN's interconversion between inhibitory and non-inhibitory topologies. Phosphorylation at Ser16 of PLN or increased [Ca^{2+}] allosterically signals a topological transition of PLN's TM domain that shifts the equilibrium toward the non-inhibitory state, thus augmenting Ca^{2+} transport and cardiac

contractility. This intramembrane regulatory mechanism represents a potential paradigm of the structural basis of SERCA activity modulation by regulins in response to different physiological cues.

Topological equilibrium of PLN free and in complex with SERCA

In lipid membranes, PLN adopts an *L*-shaped conformation, with a membrane-adsorbed, amphipathic regulatory region (domain Ia, M1 to T17) connected by a short loop (Ile18 to Gln22) to a helical inhibitory region (domains Ib, Gln23 to Asn30; and domain II, Leu31 to Leu52), which crosses the SR membrane[19,20]. In its storage form, PLN is pentameric[20-22] and de-oligomerizes into active *L-shape* monomers[19]. The dynamic cytoplasmic region undergoes an order-disorder transition between tense (*T*) and relaxed (*R*) states, with the latter promoted by Ser16 phosphorylation[15,23,24]. Upon binding SERCA, domain Ia transitions to a more-rigid and non-inhibitory bound (*B*) state, which becomes more populated upon phosphorylation[15,24]. How Ser16 phosphorylation signals the reversal of inhibition to the TM region, however, remains unkown. Since the inhibitory TM region is ~ 45 Å away from Ser16 and ~ 20 Å from the SERCA's Ca^{2+} binding sites, we speculated that both phosphorylation (of PLN) and Ca^{2+} binding (to SERCA) must transmit conformational and topological changes across the membrane, thus allosterically modulating SERCA's function.

Residue-specific anisotropic NMR parameters such as CSs and DCs are exquisitely suited to describe topological transitions such as tilt, bend, and torque of TM proteins in lipid bilayers near-physiological conditions[25,26]. Their analysis by OS-ssNMR requires that membrane-embedded proteins are uniformly oriented relative to the static magnetic field (**B_0**). Therefore, we reconstituted PLN free and in complex with SERCA into magnetically aligned lipid bicelles[27]. Since monomeric PLN is the functional form[28], we utilized a monomeric mutant of PLN devoid of TM cysteine residues[29]. Both unphosphorylated (PLN^{AFA}) and phosphorylated ($pPLN^{AFA}$) variants of PLN were expressed recombinantly, while SERCA

was purified from mammalian tissues[30]. Since lipid bicelles orient spontaneously with the normal of the membrane ($\vec{n}$) perpendicular to $\mathbf{B_0}$, we doped the sample with Yb^{3+} ions to change the magnetic susceptibility and orient the lipid membranes with $\vec{n}$ parallel to $\mathbf{B_0}$. This expedient doubles the values of CSs and DCs and increases the resolution of the NMR spectra[31,32]. Fig. 1a shows the 2D [^{15}N-^{1}H] signal-enhanced (SE)-SAMPI4[33] separated local field (SLF) spectra of free PLN^{AFA} and $pPLN^{AFA}$. Due to PLN's intrinsic conformational dynamics, the SLF spectra visualize only its TM region. The spectra display the typical wheel-like pattern diagnostic of a helical conformation for both the TM domains of PLN^{AFA} and $pPLN^{AFA}$. Residue-specific assignments were carried out on free PLN^{AFA} using a combination of a 3D SE-SAMPI4-PDSD spectrum[34], selective ^{15}N labeled samples, and predictions from MD simulations[35] (Extended Data Table S1; Extended Data Fig. 1-3). To obtain the topology in lipid bilayer, the assigned resonances were fit to idealized *P*olar *I*ndex *S*lant *A*ngle (PISA) models extracting whole-body tilt (θ) and rotation or azimuthal (ρ) angles[36,37], which for free PLN^{AFA} was $\theta = 37.5 \pm 0.7°$ and $\rho_{L31} = 201 \pm 4°$, and for $pPLN^{AFA}$ $\theta = 34.8 \pm 0.5°$ and $\rho_{L31} = 201 \pm 4°$, where ρ_{L31} is the rotation angle referenced to Leu31. Notably, the high resolution of the oriented SLF spectra of PLN^{AFA} show two distinct sets of peaks (Fig. 1b), with populations unevenly distributed. The average population of the minor state estimated from the normalized peak intensities is approximately 30 ± 9 %. Remarkably, the resonances of the minor population overlap almost entirely with those of $pPLN^{AFA}$ (Fig. 1b), revealing a topological equilibrium in which the TM region of PLN interconverts between two energetically different orientations. We previously showed that PLN phosphorylation shifts the conformational equilibrium toward the *R* state[24], releasing the interactions with the lipid membranes of domain Ia (Fig. 1c). Our OS-ssNMR data show that these phosphorylation-induced effects propagate to the TM domains, shifting the topological equilibrium toward the less populated state. Since a similar mechanism may occur in the regulation of the ATPase, we reconstituted the SERCA/PLN complex in lipid bicelles and studied it by OS-ssNMR. To assess the

alignment of mammalian SERCA in bicelles, we cross-linked the most reactive cysteines with a trifluoromethylbenzyl (TFMB)-methanethiosulfonate (MTS) tag and probed its alignment by ^{19}F NMR (Fig. 1d and Extended Data Fig. 4). Five of the twenty-four cysteines of SERCA were uniquely labeled as monitored by solution NMR in isotropic bicelles (q = 0.5). In anisotropic bicelles (q = 4.0) and at low temperature, the ssNMR spectrum of ^{19}F-SERCA consists of a single unresolved ^{19}F resonance due to the rapid reorientation of the enzyme in the isotropic phase. Upon increasing the temperature, into the bicelle phase, the ^{19}F-SERCA/bicelle complex orients with $\vec{n}$ perpendicular to $\mathbf{B}_0$, and the ^{19}F resonance becomes anisotropic as a triplet with 1.3 kHz dipolar coupling[38]. Fig. 1e shows the 2D SLF spectra of PLN^{AFA} and pPLN^{AFA} in complex with SERCA. To maintain a functional and stable complex, we used a lipid-to-complex molar ratio of 2000:1, with PLN concentration 10 times less than in the SERCA free samples. Therefore, the signal-to-noise ratio in the oriented spectra is significantly reduced relative to the free forms. Nonetheless, the SLF spectra of both SERCA/PLN^{AFA} and SERCA/pPLN^{AFA} complexes show the wheel-like patterns typical of the α-helical domains with selective exchange broadening for resonances located at the protein-protein binding interface (Fig. 1f). The assigned peaks associated with the helical domain II were fit to the ideal PISA model, yielding $\theta = 33.2 \pm 1.2°$ and $\rho_{L31} = 193 \pm 7°$. Therefore, upon binding SERCA, PLN^{AFA} undergoes a clearly distinguishable -4.3 ± 1.4° change in tilt and a less defined -8 ± 8° change in rotation. These error bounds factor the linewidths and variation associated with substituting ambiguous assignments into the PISA fitting (parentheses of Fig. 1e). Similarly, the PISA model for pPLN^{AFA} was fit to $\theta = 30.4 \pm 1.1°$ and ρ_{L31} of 197 ± 4°, suggesting that the topology of the TM domain requires adjustments of -3.4 ± 1.2° and -4 ± 6° to form a complex with the ATPase. The upright tilt movements of the inhibitory domain II associated with phosphorylation and complex formation were accompanied by a dramatic broadening of peaks in the cluster of isotropic resonances around 140 ppm (Fig. 1e). These resonances are attributed to the dynamic domain Ib residues, and their disappearance is

consistent with SERCA binding, which requires the unwinding of the juxtamembrane region, and a concomitant reduction of the tilt angle to re-establish hydrophobic match with the thickness of the lipid bilayer[13,24]. Analysis of the SLF spectra also shows that phosphorylation of PLN at Ser16 restores the intensities of most resonances except for those at the upper binding interface (*i.e.*, Asn30, Leu31, Asn34, and Phe41). These spectral changes suggest a weakening of PLN-SERCA packing interactions, rather than a complete dissociation of the complex, which is consistent with prior MAS-ssNMR, EPR, and FRET measurements[13,24,39,40].

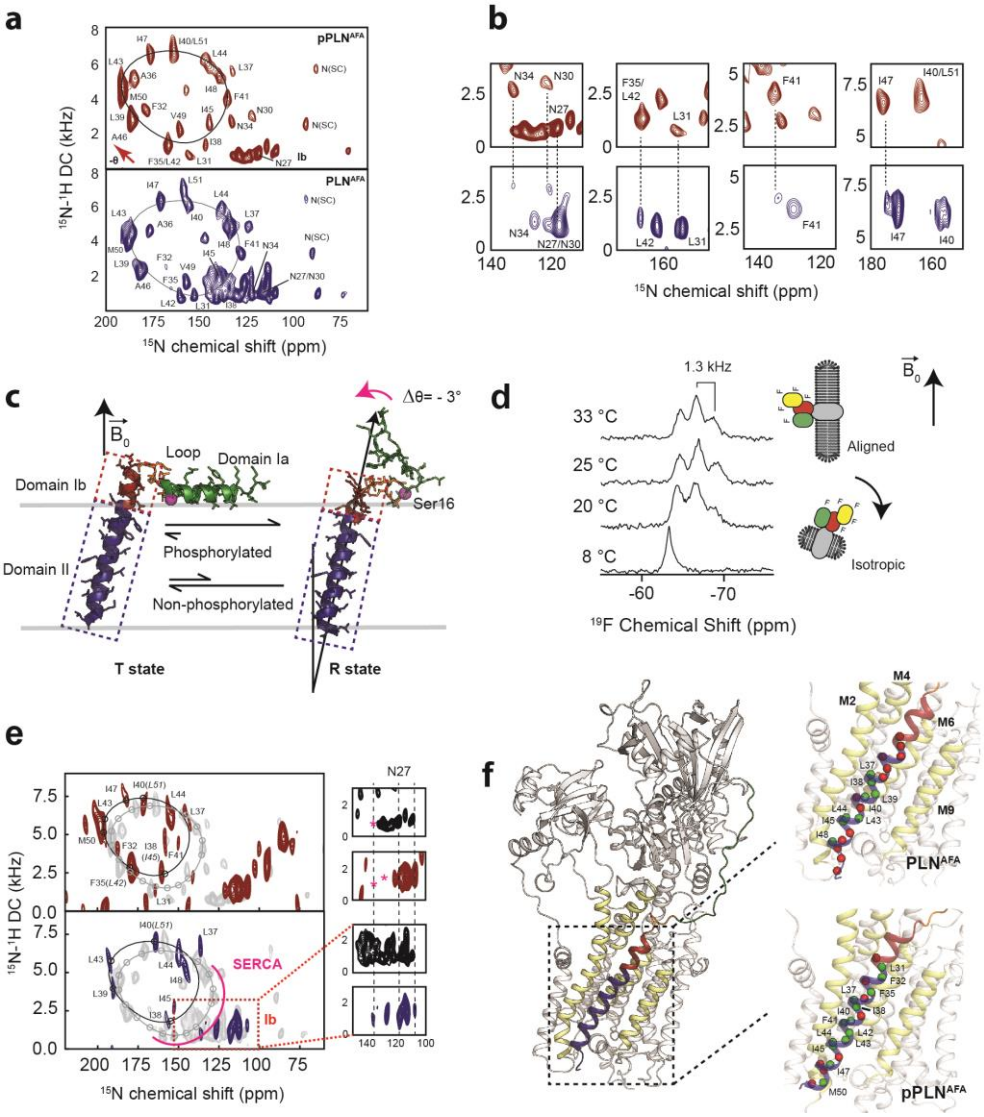

Fig. 1: Topological equilibrium of PLN and pPLN free and bound to SERCA in lipid bilayers detected by OS-ssNMR. a, 2D [^{15}N-^{1}H] SE-SAMPI4 spectra of PLN^{AFA} and pPLN^{AFA} reconstituted into aligned lipid bicelles. The fitting of resonance

patterns with PISA wheels for an ideal helix [(ϕ, ψ)=(-63°, -42°)] is superimposed. **b,** Expanded regions of PLN^{AFA} ^{15}N-labeled at N, L, F, or I residues (lower panel, blue contours) showing two populations. The upper panels (red) are the corresponding regions for the U-^{15}N labeled $pPLN^{AFA}$. U-^{15}N labelled spectra were acquired at higher signal-to-noise to observe the second population. **c,** Structures of the *T* (PDB 2KB7[19]) and *R* (PDB 2LPF[41]) states for PLN^{AFA}. **d,** ^{19}F NMR spectra of TFMB-tagged SERCA reconstituted into anisotropic (q = 4) bicelles at variable temperatures. **e,** 2D [^{15}N-^{1}H] SE-SAMPI4 spectra of uniformly ^{15}N labeled PLN^{AFA} (blue, lower panel) and $pPLN^{AFA}$ (red, upper panel) bound to SERCA in the absence of Ca^{2+} (*E*2 state). Spectra are overlaid with PLN^{AFA} or $pPLN^{AFA}$ in their free forms (grey). PISA wheels are overlaid, showing assigned residues (black points) used to fit helical tilt and rotation angles. Ambiguous assignments are shown in parentheses. The region corresponding to domain Ib is expanded to show peak broadening (asterisk) following the transition of PLN's cytoplasmic region to the *B* state. **f,** Selected structure of the SERCA/PLN^{AFA} complex. Expanded region shows visible (green spheres, labelled) and broadened (red spheres) residues mapped onto domain II of PLN^{AFA} (left) and $pPLN^{AFA}$ (right, form a structure of the SERCA/PLN^{AFA} complex).

Dynamic structural refinement of the SERCA-PLN complexes

To determine the structural ensembles of the SERCA/PLN^{AFA} and SERCA/$pPLN^{AFA}$ complexes, we incorporated the data from our experimental measurements into RAOR-MD samplings[17,18]. This dynamic refinement methodology employs full atomic MD simulations in explicit lipid membranes and water and utilizes restraints from sparse datasets to generate experimentally-driven structural ensembles. As starting coordinates for our samplings, we used the X-ray structure of the *E*2-SERCA/PLN complex, where a super-inhibitory mutant of PLN was used for crystallization[16]. We docked the TM domains of PLN^{AFA} using restraints obtained from chemical cross-linking experiments for both cytoplasmic and luminal sites[14,42,43] (Extended Data Fig. 5a). The dynamic cytoplasmic region (loop and domain Ia), which was not resolved in the crystal structure, was held in proximity to the nucleotide-binding (N) and phosphorylation (P) domains of SERCA using boundary restraints from paramagnetic relaxation enhancements (PRE) obtained from MAS-ssNMR[24]. Additionally, CSs and DCs from OS-ssNMR were applied to the TM region as ensemble-averaged restraints across eight replicas. The resulting structural ensembles were in excellent agreement with all the available experimental data for both complexes. The overall profile of average pairwise distances from residues in domain Ia and loop to the spin-labelled Cys674 matches the PRE measurements, with the minimal distance (*i.e.* maximum PRE effect) observed for PLN-Tyr6 (Extended Data Fig. 5b,c). Similarly, back-calculated CS and DC values for PLN^{AFA} and

pPLN^{AFA} were in excellent agreement with experiments (Extended Data Fig. 5d). Average back-calculated tilt angles of 32.8° and 30.4° for PLN^{AFA} and pPLN^{AFA}, respectively, matched PISA fits to experimental values (Extended Data Fig. 5e,6). All pairwise distances between previously reported crosslinkable positions[14,42-44]were distributed within acceptable ranges (Extended Data Fig. 5f). Although not used as an initial docking restraint, cytoplasmic residues PLN Lys3 and SERCA Lys397 were also partially distributed within a distance consistent with previously reported crosslinking[45].

To assess the conformational landscape of the SERCA/PLN complexes, we used principal component analysis (PCA). PCA identified a combined opening of the cytoplasmic headpiece involving a hinge-like displacement of the N domain and rotation of the A domain away from the P domain (PC1) and planar rotations separating the N and A domains (PC2) (Fig. 2a,b, Extended Data Fig. 7, Extended Data Movie 1). These motions differentiate the *E*1 and *E*2 states of SERCA, as shown by the projections of crystal structures onto the PCA map (Fig. 2c,d). The SERCA/PLN^{AFA} complex spans four distinct clusters, while the SERCA/pPLN^{AFA} complex spans eight (see Extended Data Fig. 8 for representative structures). When bound to PLN^{AFA}, SERCA mostly retains the compact *E*1-like headpiece present in the crystal structure, which is also found for SERCA/SLN[46], and interconverts with equal frequency between a highly compact cluster (3) resembling nucleotide-bound *E*1 states and a cluster (1) intermediate toward the *E*2 states, which exhibits a partial opening of the A and N domains caused by breaking of the salt bridges involving Arg139-Asp426/Glu435 and Lys218-Asp422. Similar states were also present with pPLN^{AFA}, but the interaction of pSer16 with Arg604 weakens the Asp601-Thr357 and Arg604-Leu356 hydrogen bonds at the hinge of the N and P domains, leading to four additional open states (clusters 5 to 8). Separate clusters correspond to successive breakages of interdomain hydrogen bonds in the headpiece. Salt bridges between PLN-Ser16 to SERCA-Arg460 and PLN-Arg14 to SERCA-Glu392 were also found to stabilize these open states (Extended Data Fig. 9). These open states resemble off-pathway crystal

structures solved for the Ca_2E1 state observed in the absence of nucleotide[7,47,48]. For all clusters, the binding at PLN-Ser16 was more defined for SERCA/pPLN^{AFA} than for the non-phosphorylated complex (Fig. 2e,f, Extended Data Fig. 8).

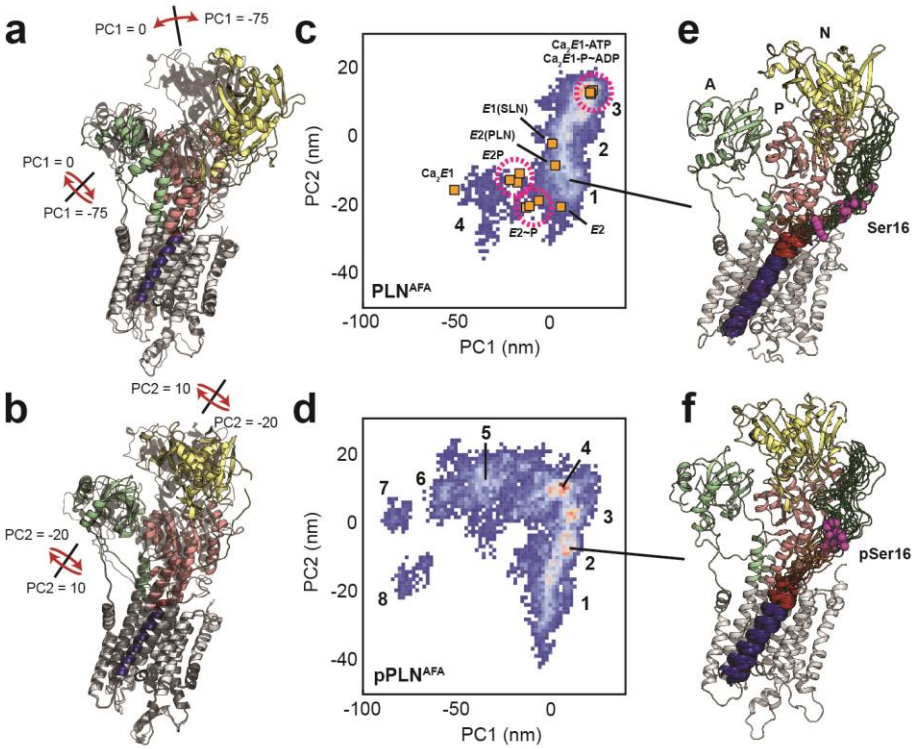

Fig. 2: Conformational landscape of SERCA/PLN^{AFA} and SERCA/pPLN^{AFA} complexes. a, b, Depiction of headpiece movements associated with the first (**a**) and second (**b**) principal components. Structures with the highest PC values are shown as transparent black. **c, d,** PCA histograms of SERCA/PLN^{AFA} (**c**) and SERCA/pPLN^{AFA} (**d**) structural ensembles with projections of crystal structures in various states: Ca_2E1-ATP[49,50], Ca_2E1~P-ADP[50-52], Ca_2E1[47], $E1$-SLN[46], $E2$-PLN[16], $E2P$[51,53], $E2$~P[51,53,54], and $E2$[55]. Clusters are numbered. **e,** f, Top 20 most representive structures of PLN^{AFA} (**e**, cluster 1) and pPLN^{AFA} (**f**, cluster 2) bound to SERCA from the most representative state.

From the analysis of the structural ensembles of the two complexes, it emerges that the relief of inhibition occurs via a rearrangement of the intramembrane contacts between the TM region of pPLN^{AFA} and SERCA, with a reconfiguration of electrostatic interactions near the phosphorylation site and a disruption of packing at the protein-protein interface (Fig. 3a,b). The interactions between the cytoplasmic region are transient and highly dynamic. For both complexes, we observed persistent interactions between PLN-Glu2 and SERCA-Lys365, PLN-Glu19, and SERCA-Lys328, and to a lesser extent PLN-Lys3 and

SERCA-Asp399 and PLN-Tyr6 and SERCA-Asp557. For PLN^{AFA}, however, the arginine residues (Arg9, Arg13, and Arg14) interacted transiently with SERCA-Glu606, while for $pPLN^{AFA}$, the phosphate group at Ser16 interacts strongly with SERCA-Arg604 and SERCA-Lys605. Interestingly, we detected the formation of intramolecular salt-bridges between the phosphate of Ser16 and PLN-Arg9, PLN-Arg13, and PLN-Arg14, causing domain Ia to adopt a compact conformation as previously suggested by fluorescence data[56,57] (Extended Data Table 2, 3). These conformational transitions sever intermolecular contacts of PLN's domain Ib and SERCA's TM helices involving Gln23-Leu321/Arg325 (M4), Lys27-Phe809 (M6) and Asn30-Trp107 (M2), weakening the inhibitory interactions (Fig. 3a and Extended Data Fig. 10). In fact, hydrophobic substitutions at these positions have been identified as hotspots for engineering superinhibitory PLN mutants (*i.e.*, Asn/Lys27Ala and Asn30Cys), which exhibit stable helical structure well into the loop domain[16,58,59]. Destabilization and detachment of this region is consistent with the reappearance of exchange-broadened interfacial resonances of domain II paralleled by broadening of the resonances of the dynamic domain Ib in the SLF spectra of the SERCA/$pPLN^{AFA}$ complex (Fig 1e). For both complexes, the electrostatic interactions of PLN-Arg13, PLN-Arg14, or PLN-pSer16 with the SERCA's Arg604 -Glu606 stretch cause the detachment of PLN's domain Ib and the consequent weakening of the inhibitory interaction (Fig. 3c-f). This illustrates the regulatory role of the *B* state of PLN for relieving inhibition and the superinhibitory activity of domain Ia-truncated PLN[24].

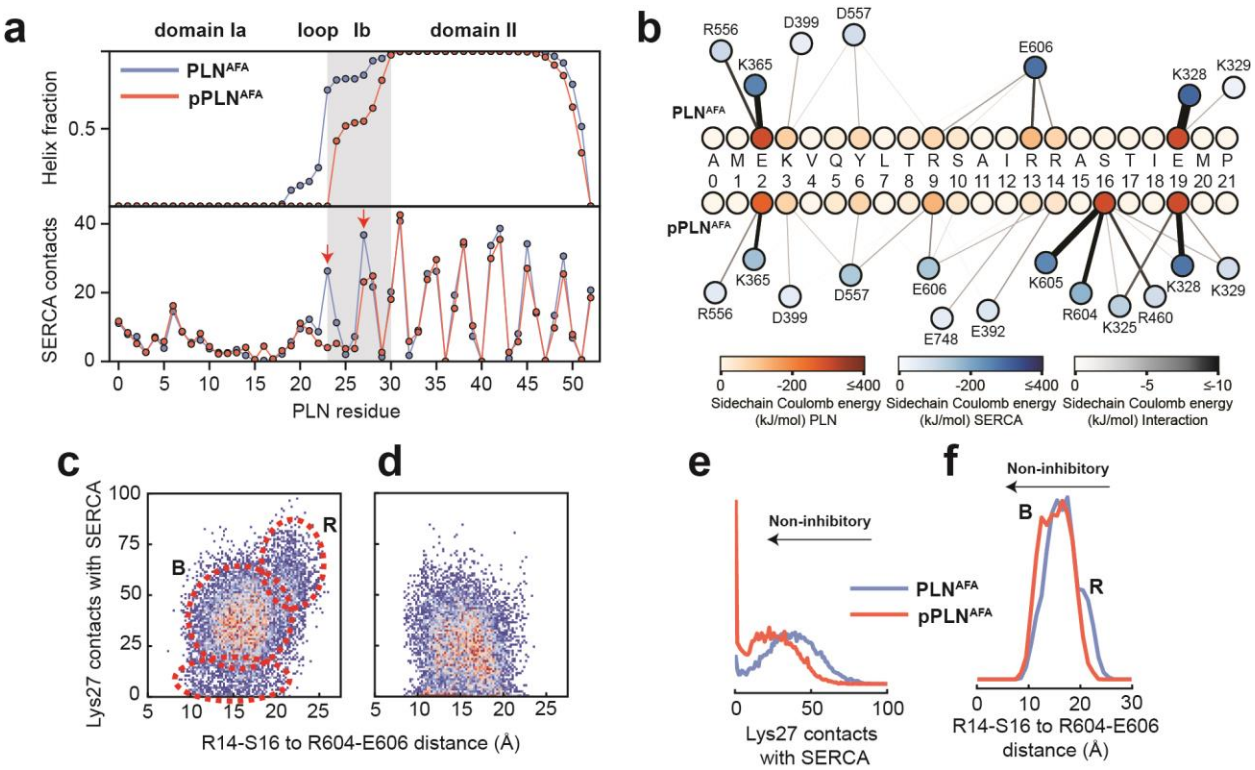

Fig. 3. Mechanism for reversal of PLN inhibition by phosphorylation. a, Ensemble-averaged per-residue structural analysis (upper panel) and intermolecular contact profiles (lower panel). A contact is defined when any PLN atom comes within 3.5 Å of any SERCA atom for any given frame. **b,** Spider plot of pairwise electrostatic interactions between cytoplasmic residues and SERCA in RAOR-MD ensembles. **c, d,** 2D Histograms correlating the distances between the cytoplasmic binding interfaces, defined by the center of masses of Arg14 to Ser16 of PLN and Arg604 to Glu606 of SERCA, to the inhibitory intermolecular contacts of PLN Lys27 for the SERCA/PLN^{AFA} (**c**) and SERCA/pPLN^{AFA} (**d**) ensembles. **e, f,** Corresponding 1D histograms for Lys27 contacts (**e**) and binding of the cytoplasmic domain (**f**).

To assess the effects of PLN on Ca^{2+} transport, we calculated the correlations between PLN's topological changes and the corresponding variations of SERCA's TM domain (Fig. 4a-d). When PLN^{AFA} is bound to SERCA, we observe a dense network of correlated motions between PLN's TM region and the binding groove (TM2, TM6, and TM9), as well as a dense cluster of correlations involving TM3, TM4, TM5, TM6, and TM7. This allosteric coupling influences the geometry of the Ca^{2+} binding sites, possibly reducing the Ca^{2+} binding affinity of SERCA. In contrast, pPLN^{AFA} bound to SERCA displays correlated motions only with the most proximal SERCA helices, while the dense network of correlations involving TM4, TM5, TM6, and TM8 is sparse and rearranged. Overall, phosphorylation of PLN at Ser16 increases the electrostatic interactions with the cytoplasmic domain of SERCA (*R* to *B* state transition, *i.e.*, disorder

to order)[24], which simultaneously weakens intramembrane protein-protein interactions to uncouple the dynamic transitions of PLN from SERCA and remove its structural hindrance against Ca^{2+} transport (Fig. 4e,f).

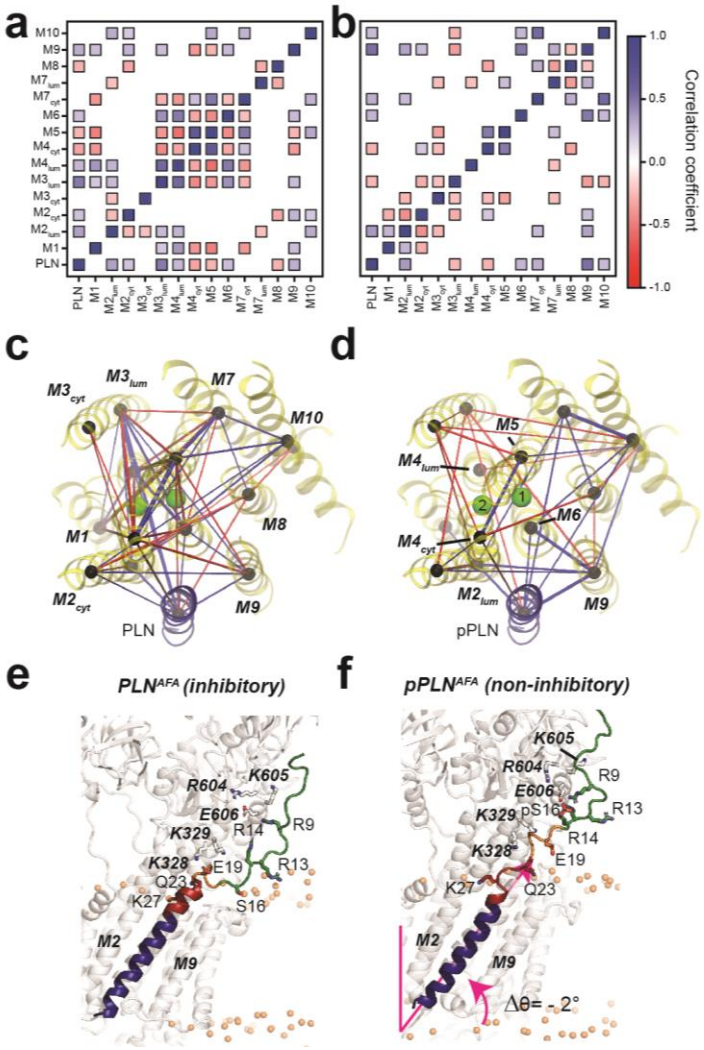

Fig.4. PLN topological transitions are allosterically coupled to SERCA's conformational states. a, b, Correlation maps of motions between the TM topology of PLN^{AFA} (**a**) or $pPLN^{AFA}$ (**b**) with the topology of the 10 TM domains of SERCA. **c, d,** Corresponding spider plots showing the density of correlations are displayed below. Positions of the calcium binding sites are marked by green spheres. **e, f,** Snapshots of the SERCA/PLN^{AFA} (**e**) and SERCA/$pPLN^{AFA}$ (**f**) complexes highlighting the transient interactions with the cytoplasmic region and loosened interactions with the TM region of SERCA.

Effects of Ca^{2+} ion binding to SERCA on PLN's topological equilibrium

To assess the effects of Ca^{2+} on SERCA regulation, we performed SLF experiments on PLN^{AFA} and $pPLN^{AFA}$ complexed with SERCA in the *E*1 state (Fig. 5a-d). Addition of Ca^{2+} to the SERCA/PLN^{AFA} complex did not cause significant changes to the PLN topology ($\theta = 32.9 \pm 1.4°$ and $\rho_{L31} = 199 \pm 4°$), but the intensity of the resonances in the spectra indicate a reconfiguration of the binding interface, with the reappearance of PLN resonances for Phe32, Phe35/Leu42 and Ala36. Distinguishable topological changes, however, are observed for the SERCA/$pPLN^{AFA}$ complex, for which Ca^{2+}-binding induced a decrease of both tilt and rotational angles of $1.8 \pm 1.3°$ and $10 \pm 7°$, respectively ($\theta = 28.6 \pm 0.7°$ and $\rho_{L31} = 187 \pm 6°$). Due to the lack of X-ray structures, we were unable to carry out dynamic modeling of these complexes. However, these experimental results suggest that Ca^{2+} binding to SERCA is allosterically coupled with PLN's topology, and this effect depends on the phosphorylation state of PLN. Similar to the effects of PLN phosphorylation on the *E*2 state of SERCA, the relief of inhibition by Ca^{2+} occurs via changes in tilt and azimuthal angles that reconfigure intramembrane inhibitory interactions.

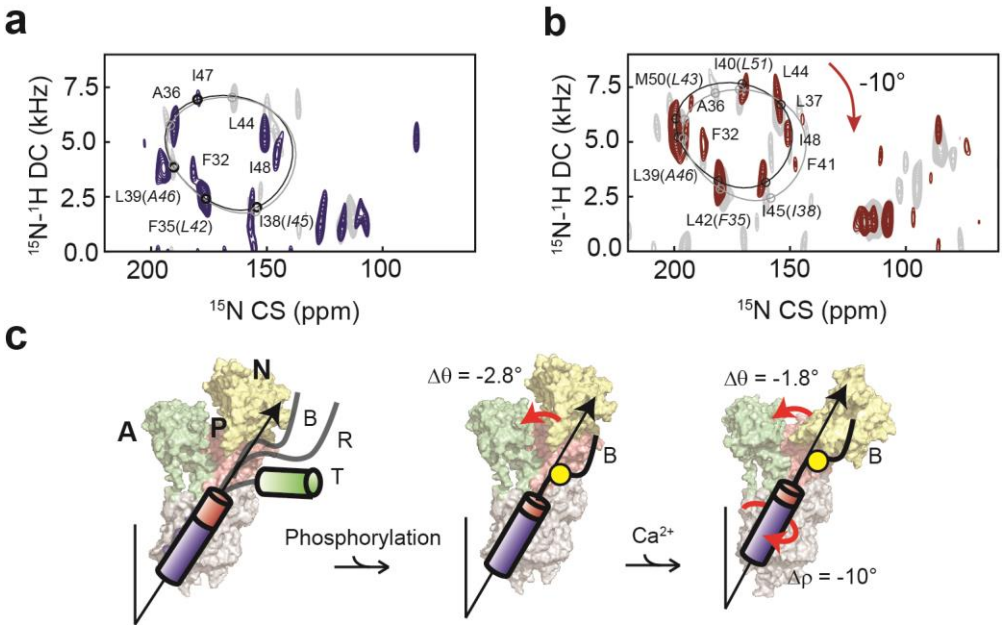

Fig. 5: Effects of Ca^{2+} binding to SERCA on the topology of PLN and pPLN. a, b, 2D [^{15}N-^{1}H] SE-SAMPI4 spectrum of PLN^{AFA} (**a**) and $pPLN^{AFA}$ (**b**) bound to SERCA in the *E*1 form reconstituted into aligned lipid bicelles. PISA wheels for an ideal helix [(ϕ, ψ)=(-63°, -42°)] are superimposed. Equivalent spectra of the *E*2 form complexes are shown in grey. **c,** The conformational and topoplogical effects of phosphorylation and Ca^{2+} binding to the SERCA/PLN^{AFA} complex.

Recent X-ray investigations and extensive computational studies showed that SERCA undergoes significant rocking motions throughout its enzymatic cycle[60-62]. These conformational transitions analyzed in the absence of PLN are highly concerted and cooperative, *i.e.*, the dynamics of the cytoplasmic headpiece of SERCA correlates with that of its TM domains[61,62]. Indeed, OS-ssNMR data revealed that PLN's topology is coupled to the conformational dynamics of SERCA. Remarkably, in addition to localized disruption of PLN domain Ib contacts, phosphorylation and Ca^{2+}-binding signal a collective switch of PLN's TM domain from an inhibitory to a non-inhibitory topology. Tilt angle reductions of PLN accompanying the relief of inhibition were easily measured by OS-ssNMR, while rotations were substantially more difficult to detect, but on the order of 10°, would be sufficient to disrupt critical inhibitory interactions (Fig. 6). Topological transitions, therefore, provide lever-like, and potentially rotary dial-like, mechanisms to modulate TM protein-protein interactions, which can be tuned by the conformational dynamics, posttranslational modification and binding of extramembrane regulatory sites. These topological interconversions of PLN, detected by OS-ssNMR, resolves an ongoing controversy about the *subunit* vs. *dissociative* models proposed for SERCA regulation[9,39,40,63,64]. The latter models speculate that the reversal of the inhibitory function of PLN is due to a complete dissociation of this regulin from the ATPase; but this is not supported by spectroscopic data either *in vitro* or *in cell*[13,24,39,40,64]. On the other hand, the subunit model agrees well with all spectroscopic measurements, but it does not explain the reversal of inhibition caused by phosphorylation or the elevation of Ca^{2+} concentration. Our ssNMR-driven dynamic modeling clearly shows that topological changes modify the interactions at the interface and are propagated to the distal Ca^{2+} binding sites. In this framework, it is possible to explain how single-

site disease mutations in domains Ia and Ib may lead to perturbations of the protein-protein electrostatic network of interactions, resulting in dysfunctional Ca^{2+} transport[58,65,66].

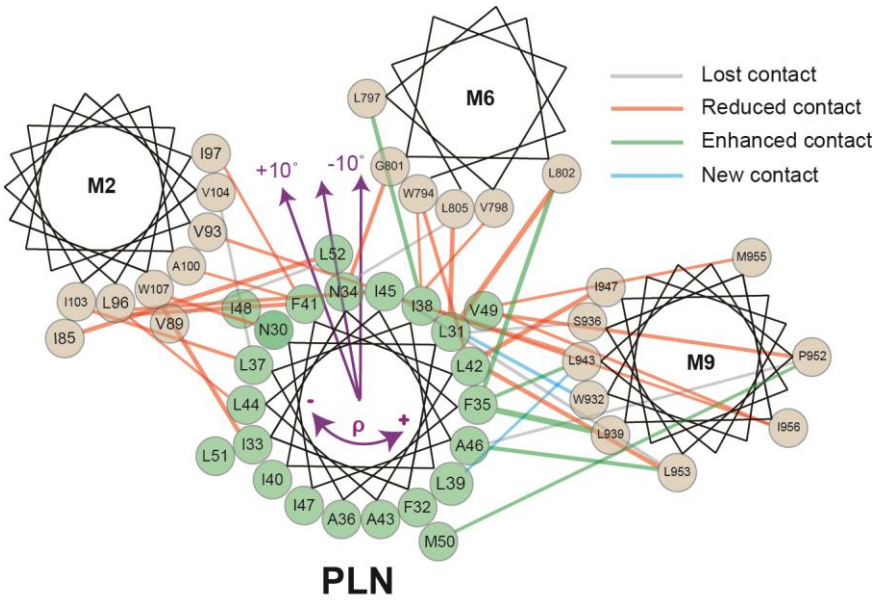

Fig. 6. Reconfiguration of SERCA/PLN TM interactions upon phosphorylation. Inhibitory pairwise interactions that were disrupted in RAOR-MD ensembles of the phosphorylated complex. Directions of the arrows exemplify clockwise or counterclockwise rotations of the TM domain of PLN.

Overall, the *topological allostery* identified for PLN may explain how bitopic miniproteins, despite their simple architecture, can fulfill diverse regulatory roles and how posttranslational modification at cytoplasmic sites may constitute switches for signal transduction across cellular membranes operated by single or multiple transmembrane domains[67]. Several mini-membrane proteins regulate membrane-embedded enzymes or receptors[1]. In the heart, phospholemman[68-70], a member of the FXYD family, regulates the Na^+/K^+-ATPase interacting via its transmembrane domain, with its regulatory interactions modulated by protein kinases A and C. Several cardiac regulins have also been recently found to control SERCA's isoforms in other tissues[2]. These mini-proteins share high homology and similar topologies, including that of PLN. They all bind at distal locations from the active sites (e.g., ATP or ion channels) of enzymes, revealing possible hot-spots for allosteric control by small molecules. Therefore, the characterization of the topological allosteric control of SERCA by PLN represents a first step in

understanding how and why evolution has preserved these small polypeptides as a means to regulate the function of ATPases[69,71] or other membrane transporters[72].

Acknowledgments

This work was supported by the National Institute of Health grants R01 GM064742 and R01 HL144100 to G.V. and R01HL139065 and R37AG026160 to D.D.T. and R.L.C. D.W. was supported by an American Heart Association Postdoctoral Fellowship (19POST34420009).

References

1 Andrews, S. J. & Rothnagel, J. A. Emerging evidence for functional peptides encoded by short open reading frames. *Nat. Rev. Genet.* **15**, 193-204, (2014).

2 Anderson, D. M. *et al.* Widespread control of calcium signaling by a family of SERCA-inhibiting micropeptides. *Sci. Signal.* **9**, ra119-ra119, (2016).

3 Ma, J. *et al.* Discovery of human sORF-encoded polypeptides (SEPs) in cell lines and tissue. *J. Proteome Res.* **13**, 1757-1765, (2014).

4 Slavoff, S. A. *et al.* Peptidomic discovery of short open reading frame–encoded peptides in human cells. *Nat. Chem. Biol.* **9**, 59-64, (2013).

5 Tada, M., Ohmori, F., Yamada, M. & Abe, H. Mechanism of the stimulation of Ca2+-dependent ATPase of cardiac sarcoplasmic reticulum by adenosine 3':5'-monophosphate-dependent protein kinase. Role of the 22,000-dalton protein. *J. Biol. Chem.* **254**, 319-326, (1979).

6 Bers, D. M. Cardiac excitation–contraction coupling. *Nature* **415**, 198-205, (2002).

7 Dyla, M., Kjærgaard, M., Poulsen, H. & Nissen, P. Structure and Mechanism of P-Type ATPase Ion Pumps. *Annu. Rev. Biochem.* **89**, 583-603, (2020).

8 Ferrington, D. A., Yao, Q., Squier, T. C. & Bigelow, D. J. Comparable levels of Ca-ATPase inhibition by phospholamban in slow-twitch skeletal and cardiac sarcoplasmic reticulum. *Biochemistry* **41**, 13289-13296, (2002).

9 MacLennan, D. H. & Kranias, E. G. Phospholamban: a crucial regulator of cardiac contractility. *Nat. Rev. Mol. Cell Biol.* **4**, 566-577, (2003).

10 Chu, G. *et al.* A single site (Ser16) phosphorylation in phospholamban is sufficient in mediating its maximal cardiac responses to β-agonists. *J. Biol. Chem.* **275**, 38938-38943, (2000).

11 Segrest, J. P., De Loof, H., Dohlman, J. G., Brouillette, C. G. & Anantharamaiah, G. M. Amphipathic helix motif: Classes and properties. *Proteins: Structure, Function, and Bioinformatics* **8**, 103-117, (1990).

12 James, Z. M., McCaffrey, J. E., Torgersen, K. D., Karim, C. B. & Thomas, D. D. Protein-protein interactions in calcium transport regulation probed by saturation transfer electron paramagnetic resonance. *Biophys. J.* **103**, 1370-1378, (2012).

13 Karim, C. B., Zhang, Z., Howard, E. C., Torgersen, K. D. & Thomas, D. D. Phosphorylation-dependent Conformational Switch in Spin-labeled Phospholamban Bound to SERCA. *J. Mol. Biol.* **358**, 1032-1040, (2006).

14 Toyoshima, C. *et al.* Modeling of the inhibitory interaction of phospholamban with the Ca2+ ATPase. *Proc. Natl. Acad. Sci. USA* **100**, 467-472, (2003).

15 Seidel, K. *et al.* Structural characterization of Ca2+-ATPase-bound phospholamban in lipid bilayers by solid-state nuclear magnetic resonance (NMR) spectroscopy. *Biochemistry* **47**, 4369-4376, (2008).

16 Akin, B. L., Hurley, T. D., Chen, Z. & Jones, L. R. The Structural Basis for Phospholamban Inhibition of the Calcium Pump in Sarcoplasmic Reticulum. *J. Biol. Chem.* **288**, 30181-30191, (2013).

17 De Simone, A., Mote, K. R. & Veglia, G. Structural Dynamics and Conformational Equilibria of SERCA Regulatory Proteins in Membranes by Solid-State NMR Restrained Simulations. *Biophys. J.* **106**, 2566-2576, (2014).

18 Sanz-Hernández, M., Vostrikov, V. V., Veglia, G. & De Simone, A. Accurate Determination of Conformational Transitions in Oligomeric Membrane Proteins. *Sci. Rep.* **6**, 23063-23063, (2016).

19 Traaseth, N. J. *et al.* Structure and topology of monomeric phospholamban in lipid membranes determined by a hybrid solution and solid-state NMR approach. *Proc. Natl. Acad. Sci. USA* **106**, 10165-10170, (2009).

20 Verardi, R., Shi, L., Traaseth, N. J., Walsh, N. & Veglia, G. Structural topology of phospholamban pentamer in lipid bilayers by a hybrid solution and solid-state NMR method. *Proc. Natl. Acad. Sci. USA* **108**, 9101-9106, (2011).

21 Vostrikov, V. V., Mote, K. R., Verardi, R. & Veglia, G. Structural dynamics and topology of phosphorylated phospholamban homopentamer reveal its role in the regulation of calcium transport. *Structure* **21**, 2119-2130, (2013).

22 Mravic, M. *et al.* Packing of apolar side chains enables accurate design of highly stable membrane proteins. *Science* **363**, 1418-1423, (2019).

23 Gustavsson, M., Traaseth, N. J. & Veglia, G. Probing ground and excited states of phospholamban in model and native lipid membranes by magic angle spinning NMR spectroscopy. *Biochim. Biophys. Acta* **1818**, 146-153, (2012).

24 Gustavsson, M. *et al.* Allosteric regulation of SERCA by phosphorylation-mediated conformational shift of phospholamban. *Proc. Natl. Acad. Sci. USA* **110**, 17338-17343, (2013).

25 Opella, S. J. & Marassi, F. M. Structure Determination of Membrane Proteins by NMR Spectroscopy. *Chem. Rev.* **104**, 3587-3606, (2004).

26 Das, N., Murray, D. T. & Cross, T. A. Lipid bilayer preparations of membrane proteins for oriented and magic-angle spinning solid-state NMR samples. *Nat. Protoc.* **8**, 2256-2270, (2013).

27 Sanders, C. R. & Landis, G. C. Reconstitution of Membrane Proteins into Lipid-Rich Bilayered Mixed Micelles for NMR Studies. *Biochemistry* **34**, 4030-4040, (1995).

28 Zvaritch, E. *et al.* The Transgenic Expression of Highly Inhibitory Monomeric Forms of Phospholamban in Mouse Heart Impairs Cardiac Contractility. *J. Biol. Chem.* **275**, 14985-14991, (2000).

29 Karim, C. B., Marquardt, C. G., Stamm, J. D., Barany, G. & Thomas, D. D. Synthetic null-cysteine phospholamban analogue and the corresponding transmembrane domain inhibit the Ca-ATPase. *Biochemistry* **39**, 10892-10897, (2000).

30 Stokes, D. L. & Green, N. M. Three-dimensional crystals of CaATPase from sarcoplasmic reticulum. Symmetry and molecular packing. *Biophys. J.* **57**, 1-14, (1990).

31 Prosser, R. S., Hunt, S. A., DiNatale, J. A. & Vold, R. R. Magnetically Aligned Membrane Model Systems with Positive Order Parameter: Switching the Sign of Szz with Paramagnetic Ions. *J. Am. Chem. Soc.* **118**, 269-270, (1996).

32 Prosser, R. S., Volkov, V. B. & Shiyanovskaya, I. V. Novel Chelate-Induced Magnetic Alignment of Biological Membranes. *Biophys. J.* **75**, 2163-2169, (1998).

33 Gopinath, T. & Veglia, G. Sensitivity enhancement in static solid-state NMR experiments via singleand multiple-quantum dipolar coherences. *J. Am. Chem. Soc.* **131**, 5754-5756, (2009).

34 Mote, K. R. *et al.* Multidimensional oriented solid-state NMR experiments enable the sequential assignment of uniformly 15N labeled integral membrane proteins in magnetically aligned lipid bilayers. *J. Biomol. NMR* **51**, 339-346, (2011).

35 Weber, D. K. & Veglia, G. A Theoretical Assessment of the Structure Determination of Multi-Span Membrane Proteins by Oriented Sample Solid-State NMR Spectroscopy. *Aust. J. Chem.* **73**, 246-251, (2019).

36 Denny, J. K., Wang, J., Cross, T. A. & Quine, J. R. PISEMA powder patterns and PISA wheels. *J. Magn. Reson.* **152**, 217-226, (2001).

37 Marassi, F. M. & Opella, S. J. A Solid-State NMR Index of Helical Membrane Protein Structure and Topology. *J. Magn. Reson.* **144**, 150-155, (2000).

38 Glaser, R. W., Sachse, C., Dürr, U. H. N., Wadhwani, P. & Ulrich, A. S. Orientation of the antimicrobial peptide PGLa in lipid membranes determined from 19F-NMR dipolar couplings of 4-CF3-phenylglycine labels. *J. Magn. Reson.* **168**, 153-163, (2004).

39 Dong, X. & Thomas, D. D. Time-resolved FRET reveals the structural mechanism of SERCA-PLB regulation. *Biochem. Biophys. Res. Commun.* **449**, 196-201, (2014).

40 Bidwell, P., Blackwell, D. J., Hou, Z., Zima, A. V. & Robia, S. L. Phospholamban binds with differential affinity to calcium pump conformers. *J. Biol. Chem.* **286**, 35044-35050, (2011).

41 De Simone, A. *et al.* Structures of the Excited States of Phospholamban and Shifts in Their Populations upon Phosphorylation. *Biochemistry* **52**, 6684-6694, (2013).

42 Chen, Z., Akin, B. L., Stokes, D. L. & Jones, L. R. Cross-linking of C-terminal residues of phospholamban to the Ca2+ pump of cardiac sarcoplasmic reticulum to probe spatial and functional interactions within the transmembrane domain. *J. Biol. Chem.* **281**, 14163-14172, (2006).

43 Chen, Z., Stokes, D. L., Rice, W. J. & Jones, L. R. Spatial and Dynamic Interactions between Phospholamban and the Canine Cardiac Ca2+ Pump Revealed with Use of Heterobifunctional Cross-linking Agents. *J. Biol. Chem.* **278**, 48348-48356, (2003).

44 Jones, L. R., Cornea, R. L. & Chen, Z. Close Proximity between Residue 30 of Phospholamban and Cysteine 318 of the Cardiac Ca2+ Pump Revealed by Intermolecular Thiol Cross-linking. *J. Biol. Chem.* **277**, 28319-28329, (2002).

45 James, P., Inui, M., Tada, M., Chiesi, M. & Carafoli, E. Nature and site of phospholamban regulation of the Ca2+ pump of sarcoplasmic reticulum. *Nature* **342**, 90-92, (1989).

46 Winther, A.-M. L. *et al.* The sarcolipin-bound calcium pump stabilizes calcium sites exposed to the cytoplasm. *Nature* **495**, 265-269, (2013).

47 Toyoshima, C., Nakasako, M., Nomura, H. & Ogawa, H. Crystal structure of the calcium pump of sarcoplasmic reticulum at 2.6 A resolution. *Nature* **405**, 647-655, (2000).

48 Jensen, A. M., Sorensen, T. L., Olesen, C., Moller, J. V. & Nissen, P. Modulatory and catalytic modes of ATP binding by the calcium pump. *EMBO J.* **25**, 2305-2314, (2006).

49 Toyoshima, C. & Mizutani, T. Crystal structure of the calcium pump with a bound ATP analogue. *Nature* **430**, 529-535, (2004).

50 Sorensen, T. L., Moller, J. V. & Nissen, P. Phosphoryl transfer and calcium ion occlusion in the calcium pump. *Science* **304**, 1672-1675, (2004).

51 Olesen, C. *et al.* The structural basis of calcium transport by the calcium pump. *Nature* **450**, 1036-1042, (2007).

52 Toyoshima, C., Nomura, H. & Tsuda, T. Lumenal gating mechanism revealed in calcium pump crystal structures with phosphate analogues. *Nature* **432**, 361-368, (2004).

53 Toyoshima, C., Norimatsu, Y., Iwasawa, S., Tsuda, T. & Ogawa, H. How processing of aspartylphosphate is coupled to lumenal gating of the ion pathway in the calcium pump. *Proc. Natl. Acad. Sci. USA* **104**, 19831-19836, (2007).

54 Bublitz, M. *et al.* Ion pathways in the sarcoplasmic reticulum Ca2+-ATPase. *J. Biol. Chem.* **288**, 10759-10765, (2013).

55 Toyoshima, C. & Nomura, H. Structural changes in the calcium pump accompanying the dissociation of calcium. *Nature* **418**, 605-611, (2002).

56 Li, J., Bigelow, D. J. & Squier, T. C. Phosphorylation by cAMP-Dependent Protein Kinase Modulates the Structural Coupling between the Transmembrane and Cytosolic Domains of Phospholamban. *Biochemistry* **42**, 10674-10682, (2003).

57 Li, J., Xiong, Y., Bigelow, D. J. & Squier, T. C. Phospholamban Binds in a Compact and Ordered Conformation to the Ca-ATPase. *Biochemistry* **43**, 455-463, (2004).

58 Kimura, Y., Asahi, M., Kurzydlowski, K., Tada, M. & MacLennan, D. H. Phospholamban Domain Ib Mutations Influence Functional Interactions with the Ca2+-ATPase Isoform of Cardiac Sarcoplasmic Reticulum. *J. Biol. Chem.* **273**, 14238-14241, (1998).

59 Akin, B. L., Chen, Z. & Jones, L. R. Superinhibitory Phospholamban Mutants Compete with Ca2+ for Binding to SERCA2a by Stabilizing a Unique Nucleotide-dependent Conformational State. *J. Biol. Chem.* **285**, 28540-28552, (2010).

60 Norimatsu, Y., Hasegawa, K., Shimizu, N. & Toyoshima, C. Protein–phospholipid interplay revealed with crystals of a calcium pump. *Nature* **545**, 193-198, (2017).

61 Das, A., Rui, H., Nakamoto, R. & Roux, B. Conformational Transitions and Alternating-Access Mechanism in the Sarcoplasmic Reticulum Calcium Pump. *J. Mol. Biol.* **429**, 647-666, (2017).

62 Rui, H., Das, A., Nakamoto, R. & Roux, B. Proton Countertransport and Coupled Gating in the Sarcoplasmic Reticulum Calcium Pump. *J. Mol. Biol.* **430**, 5050-5065, (2018).

63 Mueller, B., Karim, C. B., Negrashov, I. V., Kutchai, H. & Thomas, D. D. Direct Detection of Phospholamban and Sarcoplasmic Reticulum Ca-ATPase Interaction in Membranes Using Fluorescence Resonance Energy Transfer. *Biochemistry* **43**, 8754-8765, (2004).

64 Martin, P. D., James, Z. M. & Thomas, D. D. Effect of Phosphorylation on Interactions between Transmembrane Domains of SERCA and Phospholamban. *Biophys. J.* **114**, 2573-2583, (2018).

65 Fujii, J., Maruyama, K., Tada, M. & MacLennan, D. H. Expression and site-specific mutagenesis of phospholamban. Studies of residues involved in phosphorylation and pentamer formation. *J. Biol. Chem.* **264**, 12950-12955, (1989).

66 Toyofuku, T., Kurzydlowski, K., Tada, M. & MacLennan, D. H. Amino Acids Glu2 to Ile18 in the Cytoplasmic Domain of Phospholamban Are Essential for Functional Association with the Ca2+-ATPase of Sarcoplasmic Reticulum. *J. Biol. Chem.* **269**, 3088-3094, (1994).

67 Bocharov, E. V. *et al.* Helix-helix interactions in membrane domains of bitopic proteins: Specificity and role of lipid environment. *Biochim. Biophys. Acta* **1859**, 561-576, (2017).

68 Presti, C. F., Jones, L. R. & Lindemann, J. P. Isoproterenol-induced phosphorylation of a 15-kilodalton sarcolemmal protein in intact myocardium. *J. Biol. Chem.* **260**, 3860-3867, (1985).

69 Bers, D. M., Despa, S. & Bossuyt, J. Regulation of Ca2+ and Na+ in normal and failing cardiac myocytes. *Ann. N. Y. Acad. Sci.* **1080**, 165-177, (2006).

70 Teriete, P., Thai, K., Choi, J. & Marassi, F. M. Effects of PKA phosphorylation on the conformation of the Na,K-ATPase regulatory protein FXYD1. *Biochimica et Biophysica Acta - Biomembranes* **1788**, 2462-2470, (2009).

71 Singh, D. R. *et al.* Newly Discovered Micropeptide Regulators of SERCA Form Oligomers but Bind to the Pump as Monomers. *J. Mol. Biol.* **431**, 4429-4443, (2019).

72 Makarewich, C. A. The hidden world of membrane microproteins. *Exp. Cell Res.* **388**, 111853-111853, (2020).